Engineering in Life Sciences

WILEY-VCH

Engineering in Life Sciences

RESEARCH ARTICLE OPEN ACCESS

Evaluation of 3D-Printed Resin Materials for Use in Microbial Bioprocess Applications: Suitability and Autoclavability

Carina Zierberg[1,2,3] | Marcus Leppkes[1] | Uta Bergstedt[1,3] | Mathias Ulbricht[2] | Heyko Jürgen Schultz[1,3]

[1]Faculty of Chemistry, University of Applied Sciences Niederrhein, Krefeld, Germany | [2]Chair of Technical Chemistry II, University of Duisburg-Essen, Essen, Germany | [3]Institute For Coatings and Surface Chemistry, Krefeld, Germany

Correspondence: Heyko Jürgen Schultz (heyko_juergen.schultz@hs-niederrhein.de)

Received: 5 August 2025 | **Revised:** 15 January 2026 | **Accepted:** 11 March 2026

Keywords: 3D-printing | autoclavability | biocompatibility | biotechnology | tensile strength

ABSTRACT

Three-dimensional (3D) printing technologies are continually advancing, significantly broadening their application scope. By employing fused deposition modeling (FDM) to create iterative prototypes and stereolithography (SLA) for crafting functional components, these additive manufacturing techniques offer a highly efficient solution regarding cost and production speed. Although biocompatible materials are widely accessible, the biocompatibility of resins remains a contentious issue and requires specific evaluation for the relevant microorganisms. This study investigates the use of commercially available resins for biotechnology applications in a lab environment. Special emphasis was placed on material reuse, ensuring compatibility with autoclaving, the most common sterilization technique in laboratories. An analytical assessment was performed to identify potential leaching of polymers or resin components into the surrounding medium during autoclaving and to examine whether the materials' mechanical properties are preserved post-sterilization. The outcomes of this study may promote the broader use of 3D printing in biotechnology research by highlighting its sustainability, resource-saving potential, versatility, and relevance for various laboratory applications.

Practical application: 3D printing has emerged as a crucial asset in research, highlighted by its versatility and adaptability. The application of synthetic resins in biotechnological contexts using stereolithography-based 3D printing technologies has been subject to considerable criticism in the past, primarily due to verified toxic effects. Although biocompatible resins are now commercially available, their functional performance and long-term safety have not been sufficiently studied. This study aims to facilitate the integration of 3D printing materials into standard biotechnological laboratory workflows by examining the viability of autoclaving as a sterilization technique. Additionally, for the first time, the reusability of the materials was assessed by testing their mechanical properties after multiple uses and repeated autoclaving. This approach seeks to simplify the use of 3D printing in biotechnological research, thereby facilitating its integration into routine laboratory workflows and supporting further advancements in the field.

Abbreviations: 3D, three dimensional; CAD, computer-aided design; D, inner diameter; MTP, microtiter plate; RT, Rushton Turbine; SLA, Stereolithography.

1 | Introduction

Since its inception in the 1980s—most notably marked by Chuck Hull's invention of stereolithography in 1984 - additive manufacturing technology has undergone substantial advancements, with a steadily growing range of applications [1]. It is now employed across various engineering domains, including electronics, and biomedical engineering, enabling the fabrication of components ranging from small-scale items such as dental aligners and consumer products to large-scale parts like automotive spare components [2–5]. In general, the 3D printing process follows a standardized workflow: a digital model is first created using suitable computer-aided design (CAD) software. This model is then converted into a series of discrete layers through slicing software, after which the object is fabricated layer by layer using an additive manufacturing system. Various printing technologies are employed in this context, including fused deposition modeling (FDM), selective laser sintering (SLS), and stereolithography (SLA), each differing in terms of materials used, underlying physical principles, and resulting lateral resolution. In biomedical and biotechnological applications, key requirements include high dimensional accuracy, smooth surface finishes, and, above all, the biocompatibility of the materials used [6]. In FDM, a range of thermoplastic filaments, such as polylactic acid (PLA), is available. PLA is particularly well suited for biotechnological applications due to its low cost and absence of cytotoxic components. It has already been used in the design and fabrication of entire bioreactor vessels [7]. Especially in the rapidly growing single-use sector within the bioprocessing industry, PLA has become a commonly used material for 3D-printed components. A challenge with filament-based 3D printing, particularly when using materials such as PLA, lies in the suitability of the printed parts for autoclaving. These materials do not exhibit high thermal stability, and repeated autoclaving is not recommended due to the potential for damage to the printed components [8]. Although autoclaving is not the only sterilization method, it is the most commonly used and most straightforward method, making it a significant limitation for applications where sterility and the ability to withstand multiple autoclaving cycles are critical. An alternative 3D printing method to FDM is selective laser sintering (SLS), which utilizes powdered thermoplastics such as polyamides. In biotechnology, SLS has been utilized for applications such as printing custom microtiter plates for cultivating organisms like *S. cerevisiae* [9]. However, SLS printers are relatively expensive, and the resulting parts have limited detail resolution and rough surface finishes [10, 11]. Therefore, SLS printing is primarily recommended for functional components rather than applications requiring high precision or smooth surfaces. Another possibility would be metal 3D printing, which, while promising, remains relatively expensive [12] and is therefore less suitable for smaller research laboratories. A more affordable alternative could be ceramic 3D printing [13] however, there are limitations in the precision of the printed parts, which may restrict its applicability in certain high-precision environments. The most promising 3D printing technology appears to be SLA printing with resins, which is characterized by its high precision, even for the finest parts, and relatively low acquisition and material costs. Materials produced via SLA printing have also been successfully used in technical applications such as stirrers, baffles, and other functional components, demonstrating reliable performance, and durability in these roles [14–16]. Beyond these technical uses, some resin manufacturers have developed biocompatible formulations that can withstand autoclaving, making SLA printing a highly suitable option for applications requiring both detailed resolution and material compatibility in medical or biotechnological fields.

Many studies have already investigated the biocompatibility of resins [17–19], but the applicability of these materials remains controversial and must be evaluated on a case-by-case basis, as the exact composition of commercial resins is typically kept as a trade secret. These resins are composed of monomers with methacrylate structure, which are known to exhibit cytotoxic effects [20], as well as photoinitiators, which may also contribute to cytotoxicity. An interesting approach was pursued by Musgrove et al. [21], in which 3D-printed resin models were subsequently coated with materials such as polydimethylsiloxane (PDMS) to investigate autofluorescence and biocompatibility. However, the coating process is labor-intensive and reduces flexibility in experimental design. Furthermore, it remains unclear whether the coating can withstand autoclaving. Given the complexity and limitations of post-processing steps such as PDMS coating, particularly their reduced experimental flexibility and uncertain stability during autoclaving, it is desirable to evaluate the biocompatibility of uncoated resin materials directly. In this context, the growth of *Escherichia coli*—a key organism in both industrial biotechnology and research—was investigated in test tubes fabricated from various resins, revealing growth inhibition associated with certain materials. [22]. This demonstrates that even for robust organisms such as *E. coli*, resin components may adversely affect microbial growth. For ease of use in research or routine laboratory work, autoclave compatibility is ideal; however, to the best of our knowledge, this aspect has received little attention in the scientific literature to date. The aim of this study is, therefore, also to quantitatively assess the autoclave compatibility of the materials by evaluating their mechanical properties. Furthermore, cytotoxicity toward *E. coli* will be reassessed at both small and moderately larger scales.

2 | Materials and Methods

2.1 | Modelling and Utilized Resins

All 3D printing models were designed using Autodesk Fusion CAD software (Autodesk, Inc., San Rafael, CA, USA). The additive manufacturing process utilized the Form 4 and Form 3B+ SLA printers (Formlabs, USA). Several resins were examined: Clear V4, Clear V5, Black V4, Black V5, High Temp V2, Durable V2, BioMed Clear V1, and Surgical Guide V1. According to Formlabs, the manufacturer, BioMed Clear V1 and Surgical Guide V1 resins are biocompatible and suitable for autoclaving. The eight different resins were post-processed according to the manufacturers' recommendations and cured in a FormCure (Formlabs, USA).

2.2 | Assessment of Cytotoxicity

Two different methods were used to evaluate the cytotoxicity of the 3D printing materials. All organisms were cultured in 24-well microtiter plates and assessed using a Tecan Spark 10 M

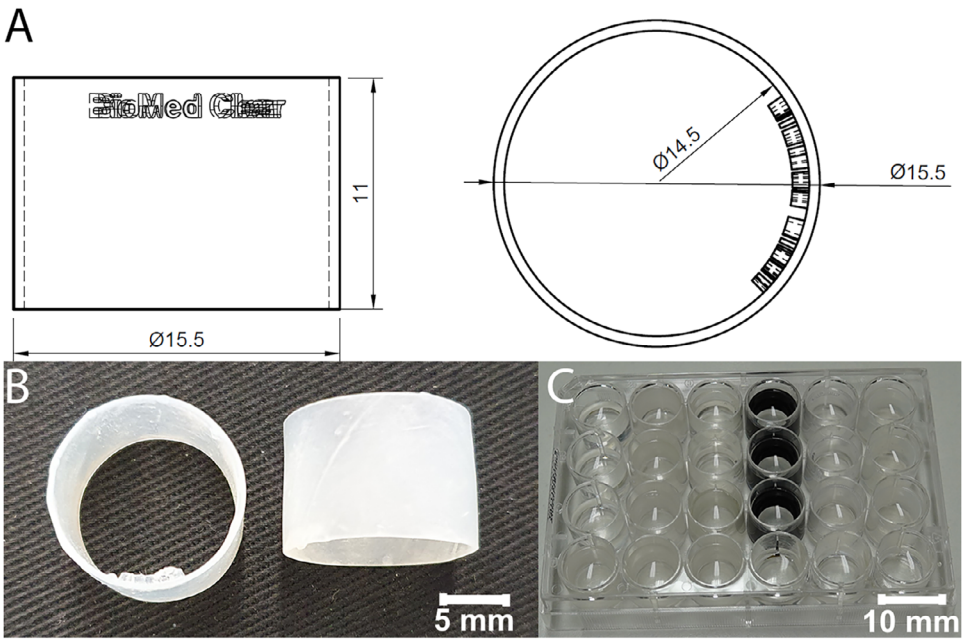

FIGURE 1 | (A) Technical drawing of the 3D-modeled rings designed to fit into a 24-well microtiter plate (dimensions in mm), (B) printed ring (Clear V4) scale bar 5 mm (derived from the known outer diameter of the ring, 15.5 mm), (C) 3D printed rings in 24-well microtiter plate, scale bar: 10 mm (derived from the standard well diameter of a 24-well plate).

plate reader (Tecan Group Ltd., Männedorf, Switzerland). To expose the organisms to the 3D-printed materials, custom-made rings (Figure 1) with a diameter of 15.5 mm were designed and printed to fit into the wells of a 24-well microtiter plate. The reference sample comprised the culture in the microtiter plate without any additives. Liquid Clear V4 resin served as a positive control.

First, native *E. coli* (DSM 498) cultures were incubated in lysogeny broth (LB) in direct contact with the test materials for 24 h, and optical density (OD) measurements at 600 nm were used to assess bacterial growth. The second approach utilized a genetically engineered strain of *E. coli* containing a *GLO* plasmid. The LB medium was supplemented with 1 g/L ampicillin and 6 g/L arabinose to induce plasmid expression. Fluorescence was measured by exciting the cells at 395 nm and recording emission at 508 nm. Native *E. coli* strain (DSM 498) served as a negative control. For all assays, a preculture was grown under identical conditions, and the main cultures were inoculated with a starting OD of 0.1.

2.3 | Tensile testing Method

The tensile tests were conducted in accordance with DIN EN ISO 527-1 and 527-2, which are commonly applied to additively manufactured (3D-printed) polymers with appropriate considerations [23, 24]. Specimen type 1BA (Figure 2, according to DIN EN ISO 527-2 [24]) was consistently used for all tests across the different 3D printing materials. To assess the autoclave resistance of the materials, the specimens were autoclaved in a VX-100 autoclave (Systec GmbH, Linden, Germany) between 0 and 10 times (121°C, 2 bar, 30 min), after which the tensile strength was measured using an AllroundLine Z050 tensile testing machine

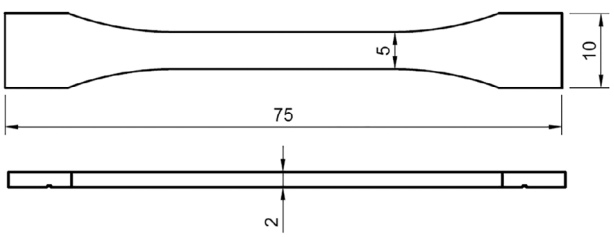

FIGURE 2 | Technical drawing of specimen type 1BA according to DIN EN ISO 527-2 (dimensions in mm).

(Zwick/Roell, Ulm, Germany). The testing speed during the tensile tests was consistently 20 mm/min.

The tensile strength σm was calculated according to the following formula:

$$\sigma_m = \frac{F}{A} \tag{1}$$

where F is the force in Newton (N) and A is the starting cross-section area in square millimeters (mm^2). The engineering strain in percent (%) was calculated according to the following formula:

$$\varepsilon = \frac{\Delta L_0}{L_0} \tag{2}$$

where L_0 is the elongation of the gauge length of the specimen in millimeters (mm) and ΔL_0 the elongation of the specimen between the gauge marks, expressed in millimetres (mm). Engineering strain at break (ε_{tb}) corresponds to the strain of the specimen at the point of fracture. Young's modulus was calculated

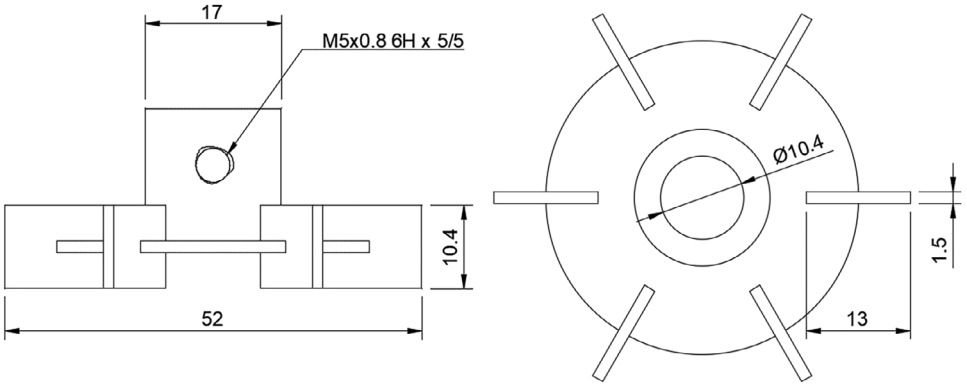

FIGURE 3 | Technical drawing of modelled Rushton Turbine with d=52 mm (all dimensions in mm).

using the regression line in accordance with DIN EN ISO 527-1 [23].

2.4 | Analysis of Leachables Released During Autoclaving

MTP rings made from the various resins described in 2.2 were placed in 1 mL of double-distilled water and autoclaved (121°C, 2 bar, 30 min) in glass snap cap vials. This procedure was repeated twice more for each material. The total organic carbon (TOC) content of the resulting water samples was analyzed using a TOC analyzer (TOC-VCPN, Shimadzu Corporation, Kyoto, Japan).

2.5 | *E. coli* Fermentations

To investigate the impact of 3D-printed components in bioreactors, replicas of standard metal Rushton turbines were fabricated (Figure 3) from the resins BioMed Clear and Surgical Guide and evaluated in an *E. coli* fermentation (Figure 9).

The fermentation was conducted in a BIOSTAT A Plus reactor system (Sartorius Stedim Biotech, Göttingen, Germany) with a working volume of 1.5 liters and an internal vessel diameter of 130 mm, operated at a cultivation temperature of 37°C (Figure 10). Aeration was supplied at a rate of 1.0 vvm via an open ring sparger with a diameter of 50 mm, equipped with fourteen holes, seven on each side, each with a diameter of 0.5 mm. Agitation was performed using a stirrer shaft fitted with two Rushton turbines (d = 52 mm). The impeller speed was automatically adjusted in response to oxygen demand, measured using an OxyFerm FDA 225 oxygen electrode (Hamilton, Bonaduz, Switzerland). The pH value was maintained at 6.8 using a pH electrode (EasyFerm Plus K8 200, Hamilton, Bonaduz, Switzerland) and controlled by automatic titration with 2 M sodium hydroxide. The composition of the medium used is summarized in Table 1. During the fermentation process, samples were collected at defined time points to monitor relevant parameters. Cell growth was assessed by measuring optical density at 600 nm (OD_{600}). Protein concentrations were determined using the Bradford assay, and lactose concentrations were quantified using the 3,5-dinitrosalicylic acid (DNS) method. After fermentation, the enzymatic activity of β-galactosidase was determined photometrically using the o-nitrophenyl-β-D-galactopyranoside (ONPG) assay. All photometric measurements were performed with a DR3900 spectrophotometer (Hach Lange GmbH, Germany).

TABLE 1 | Composition of the fermentation medium used for *Escherichia coli* cultivation.

Component	Concentration [g/L]
Ammonium chloride	1.0
Disodium hydrogen phosphate	14.6
Yeast extract	1.0
Potassium dihydrogen phosphate	3.5
Lactose	20.0
Sodium chloride	0.5
Magnesium sulfate	0.2
Peptone	0.5

3 | Results and Discussion

This study utilizes 3D printers from Formlabs, specifically the Form 3B+ for medical-grade resins such as BioMed Clear V1 and Surgical Guide V1, as well as the Form 4. Formlabs 3D printers cost around 3,000 euros, making them readily accessible for smaller research laboratories as well. The Form 4 utilizes masked stereolithography (MSLA), in which each layer is polymerized by simultaneous bottom-up exposure of the entire build area. In contrast, the Form 3B+ and earlier systems employ a laser-based stereolithography process, where the laser sequentially scans the cross-sectional geometry of each layer point by point to induce polymerization. For this reason, the question arises whether older models can be assumed to produce isotropic 3D prints, that is, whether the orientation of the models on the building platform, as well as their vertical or horizontal positioning relative to the laser, has a negligible effect on their mechanical properties. Tuteski and Kocov investigated different orientations of test specimens to examine their mechanical properties through tensile testing [25]. Their results showed that variations of up to 10% in mechanical properties can occur depending on the printing orientation. Since isotropy has not yet been investigated for the Form 4 with its novel MSLA technology, this study addressed the issue by conducting

tests using Clear V5 resin, directly compared with Clear V4 resin printed on the Form 3B+. The supporting material confirms these findings, showing deviations of up to 10% for the Form 3B+ and revealing that the mechanical properties are influenced by whether specimens are oriented horizontally or vertically relative to the laser path. The definition of specimen orientation with respect to the laser path and the MSLA technology of the Form 4 is illustrated in Figure S1, while the tensile strength results used to assess isotropic behavior are presented in Figure S2 and summarized in Table S1 (Section S1). In contrast, the Form 4 exhibited consistent results regardless of orientation, indicating a truly isotropic behavior.

Additionally, a slight decrease in tensile strength was observed with decreasing layer thickness. The corresponding experimental results are shown in Figure S3 and summarized in Table S2 (Section S2), including a comparison with manufacturer data available only for a layer thickness of 100 µm.

Furthermore, the influence of the printing orientation on the build platform itself—defined by different rotation angles in the *x*- and *y*-directions rather than the orientation relative to the laser—was investigated. The applied build-platform orientations with support structures are depicted in Figure S4, while the resulting tensile strength values are shown in Figure S5 and summarized in Table S3 (Section S3).

A comprehensive overview of all tensile testing parameters obtained for the six investigated resins after all 10 autoclaving cycles is provided in Table S4 (Section S4). For clarity, only the results corresponding to autoclaving cycles 0, 1, 5, and 10 are presented in the main text.

3.1 | Analysis of Material-Induced Cytotoxicity Using MTP Assay

The transparency of the 3D printing material is crucial, as it can otherwise interfere with the measurement of optical density. For this reason, rings were designed for the wells of a 24-well microtiter plate to ensure contact with the 3D printing material while simultaneously allowing unobstructed measurement of optical density. Additionally, a control culture was always cultivated concurrently, which was not in contact with the resins but grown solely in contact with polystyrene, the material of the microtiter plate. Liquid Clear V4 resin was used as a positive control, as unpolymerized resin is assumed to be highly toxic to the cells. The results of these initial toxicity tests, in which the growth of *E. coli* was examined, are presented in Figure 4.

The results indicate that none of the tested materials exhibit significant growth-inhibitory effects on *E. coli*. After 24 h, all cultures reached optical densities (OD) within a comparable range, indicating no substantial inhibitory effect from the tested 3D-printed materials. The control culture without exposure to any printed material reached an OD of 0.82 ± 0.01. Similar values were observed for the culture incubated with a Clear V4 ring (0.82 ± 0.02) and the BioMed Clear ring (0.78 ± 0.02). Slightly lower OD was measured for the Black V4 ring (0.77 ± 0.06), while the culture exposed to the Surgical Guide ring showed the highest OD at 0.89 ± 0.05. The observed fluctuations can be attributed

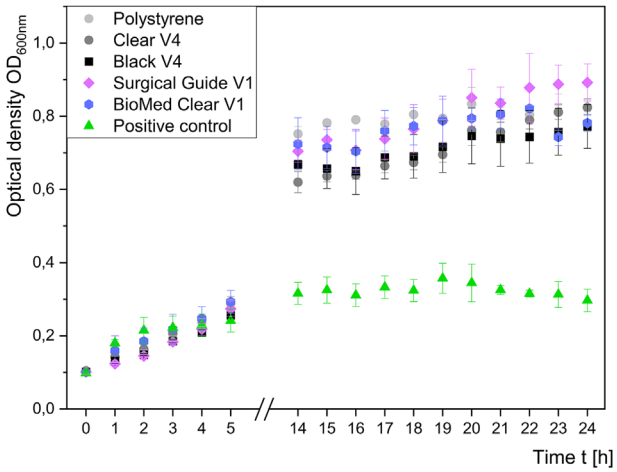

FIGURE 4 | Growth curves of *E. coli* cultures in 1 mL LB medium over a 24 h period in a 24-well microtiter plate, including a polystyrene negative control, Clear V4, Black V4, BioMed Clear V1, Surgical Guide V1, and a positive control with liquid Clear V4 resin. For each material, three replicates were measured. Error bars indicate standard deviation.

to natural variation in microbial growth. In contrast, the positive control shows an optical density of approximately 0.29 ± 0.03 after 24 h, indicating a growth-inhibitory and potentially cytotoxic effect on the cells. Initially, the positive control's optical density also appears to increase, before plateauing at around 0.2–0.3. This effect is likely due to the poor solubility of the liquid Clear resin in water, as the oily liquid naturally influences the measured optical density. In this experiment, the 3D-printed rings combined with the 1 mL culture volume resulted in a relatively high surface-to-liquid volume ratio (1071 mm^2 resin surface to 1 mL culture). Yet, the results suggest that all tested materials are suitable for cultivating *E. coli*.

Since optical density does not necessarily reflect the physiological state of the cells, and wild-type *E. coli* is known to be highly robust, a genetically modified *E. coli* strain carrying the pGLO plasmid was tested under the same conditions. Such genetically modified *E. coli* strains are widely used in research. The strain is capable of expressing green fluorescent protein (GFP), a reporter protein that fluoresces upon excitation, allowing fluorescence emission to be measured at 508 nm. A potential toxic effect would manifest in improper protein folding at the ribosomes and the formation of inclusion bodies, resulting in reduced or absent GFP fluorescence.

Black V4 resin was excluded from the fluorescence analysis, as no abnormalities were observed in the corresponding optical density measurements, and the focus of the assay was primarily on evaluating biocompatible materials. Therefore, only Clear V4 was included as a representative non-biocompatible material. As shown in Figure 5, the relative fluorescence of the cultures after 24 h of incubation was largely consistent across the tested conditions. In this context, relative fluorescence refers to the fluorescence signal normalized to the respective optical density measured for each sample. The culture exposed to Clear V4 resin exhibited a slightly more pronounced decline in fluorescence during the final 3 h compared to the control cultures. However, this effect may fall within the range of inherent biological

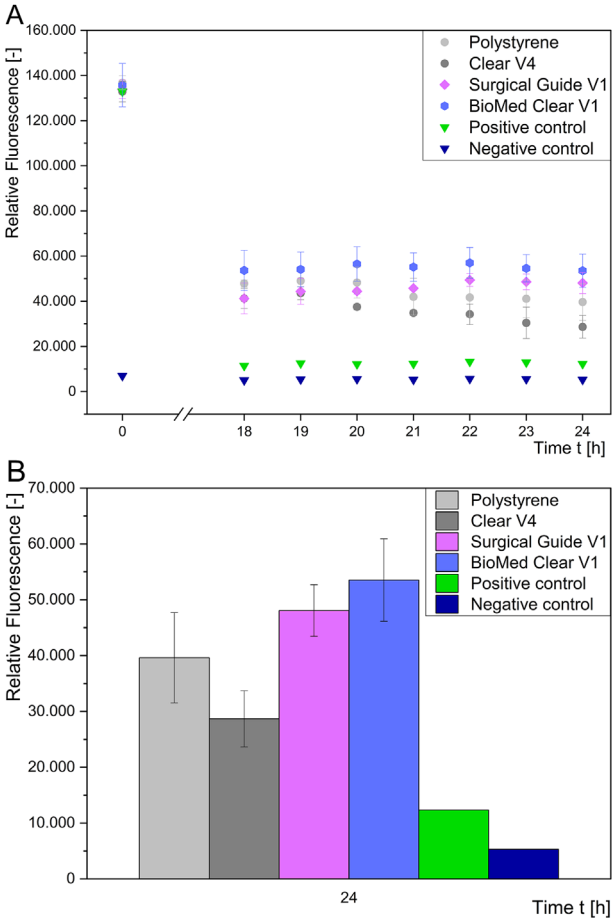

FIGURE 5 | Relative fluorescence normalized to the respective OD of *E. coli* pGLO cultures and the negative control (wild-type *E. coli*). (A) Time course of relative fluorescence over 24 h. (B) Final values after 24 h in comparison. For each material, three replicates were measured. Error bars indicate standard deviation.

variability and does not necessarily indicate a material-related influence.

The positive control, in which cells were exposed to unpolymerized Clear V4 resin, showed markedly reduced fluorescence levels as early as 18 h into the cultivation, comparable to those of the negative control (*E. coli* without the pGLO plasmid), where no fluorescence is expected.

Interestingly, after 24 h, cultures grown in the presence of BioMed Clear and Surgical Guide resins displayed slightly elevated fluorescence values compared to the polystyrene control, although this effect is not statistically significant when taking the error bars into account. Given the minor extent of this difference, it is likely attributable to inherent fluctuations in gene expression or measurement variability rather than a stimulatory effect of the materials themselves. While all wells, including the control without a ring, were shaken during incubation, the presence of the resin rings in the test wells increased the filling level on the one hand and may have introduced an additional mixing effect due to their slight movement within the wells. This minimal movement could have enhanced local mixing and oxygen transfer to the microorganisms, potentially contributing to the slightly increased optical densities and fluorescence values observed in these conditions. The general decline in fluorescence can be attributed to the decreasing availability of arabinose in the media, which induces GFP expression. The initial hours following the exposure of the cultures to the materials were also investigated but are not shown here, as the cultures were likely under significant stress. Further testing is required to verify these results but they already provide initial insights and are already meaningful with regard to the overall results of this study.

In summary, the resins labelled as biocompatible by the manufacturer appear to have no growth-inhibitory effects on either wild-type *E. coli* or genetically modified *E. coli* strains. Likewise, no significant effects were observed for the resins tested in this study, such as Clear V4 and Black V4, which are not explicitly intended for this type of application according to the manufacturer.

3.2 | Effect of Repeated Autoclaving on Tensile Properties

To assess the autoclave resistance of the tested resins, tensile tests were performed using standardized type 1BA specimens made from each material (Figure 6). Each test was repeated at least five times per material in accordance with DIN EN ISO 527-1. As polymer resins tend to become increasingly brittle with repeated heat exposure, this study limited the number of autoclaving cycles to 10. To better assess the specific effects of heat treatment during autoclaving, two additional materials were included in the test series: High Temp V2, a high-temperature resin rated by the manufacturer to withstand temperatures of up to 238°C, and Durable V2, which is formulated to tolerate higher mechanical stress. The latter was selected to evaluate whether materials designed for impact resistance maintain their mechanical integrity under the thermal and physical loads typical of autoclaving cycles. The orientation of the printed specimens was kept consistent across all prints, as shown in Figure 6. Additionally, isotropy, as well as the effects of print orientation and layer thickness, were investigated and are presented in the supporting material, which confirms up to 10% variation on the Form 3 depending on orientation, orientation-independent behavior (i.e., true isotropy) on the Form 4, and a slight decrease in tensile strength with decreasing layer thickness (Section S1, Section S2).

To initially verify the measurement method in principle with a sufficient number of different resins, a total of eight materials were subjected to the tensile test without autoclaving, and the resulting values were compared with the manufacturer's specifications. Since the agreement between our measurements and the manufacturer's specifications in most cases provided satisfactory results in a similar size range, and our measurement method even provided significantly more differentiated data, the method can be assumed to be successfully verified. The resins Black V5 and Clear V5, in combination with the Form 4 printer, were released only after the start of the experimental measurements during this study and were therefore not included in the autoclaving test series. However, based on manufacturer data, these materials do not fundamentally differ from their predecessors Black V4 and Clear V4, aside from a slightly reduced tensile strength. Due to their significantly shorter printing times, it is likely that future

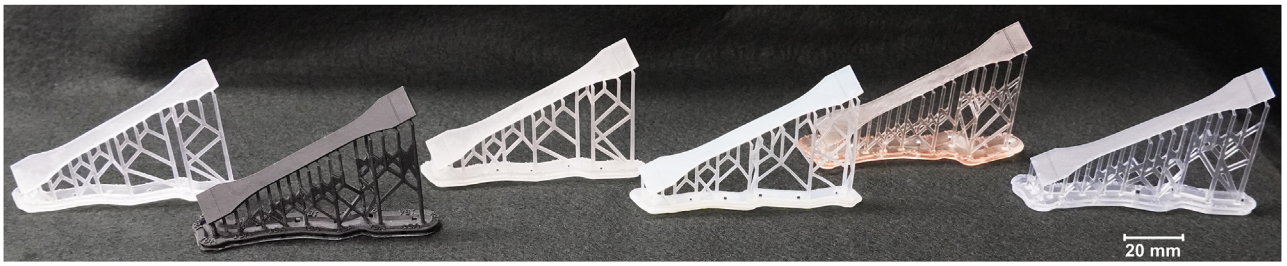

FIGURE 6 | 3D-printed type 1BA specimens, along with a supporting structure to ensure a well-defined macroscopic orientation during printing, made from various resins (from left to right: Clear V4, Black V4, High Temp V2, Durable V2, Surgical Guide V1, and BioMed Clear V1). Scale bar: 20 mm.

applications will increasingly favour the use of V5 resins. Accordingly, subsequent tests in this study were continued using selected representative materials, with Black V5 and Clear V5 excluded due to their similarity to the already tested V4 resins. The material High Temp V2 was also autoclaved and tested 10 times; however, it was surprisingly declared unsuitable for autoclaving, as the specimens became so brittle after just one autoclave cycle that tensile strength measurements were no longer feasible without restrictions. The samples were treated like all others and tested under the same conditions, but measurements on the autoclaved specimens could not always be performed.

The results of the repeated tensile tests are presented in Figure 7 with trend lines for the five remaining, suitable and selected materials (Clear V4, Black V4, Durable V2, Surgical Guide V1, BioMed Clear V1) illustrating the progression of properties over the number of cycles. Results are summarized in Table 2, which also includes values for strain and tensile modulus, as well as a comparison with the manufacturer's specifications.

Selected results of the measured tensile tests, including those for High Temp, Black V5 and Clear V5, are presented in Table 2 Where available, manufacturer specifications are also included for comparison. All the data are available in the supporting material (Section S4).

The measured tensile strength values generally show good agreement with the manufacturer's data. For Clear V4, Clear V5, and Black V4, the measured tensile strength data are higher than those specified by the manufacturers (by 20.7%, 21.2%, and 8.6%). The tensile strength of Clear V4 decreases by 15.9% after one autoclaving cycle (see Figure 7). In contrast, Black V4 retains a relatively constant tensile strength (see Figure 7), which remains in good agreement with the manufacturer's value even after 10 autoclaving cycles.

As previously mentioned, autoclaving of high temp material was not feasible due to the specimens becoming very brittle, making tensile testing nearly impossible as the samples fractured prematurely. The tensile strength determined after five autoclaving cycles showed a significant decrease compared to the unautoclaved condition. The strain at break also decreased, indicating increased brittleness. For these reasons, the process was cancelled after five autoclaving cycles for this material.

The tensile strength of Surgical Guide V1 remains relatively stable for up to five autoclaving cycles, but then decreases sharply, with an 11.4% drop observed between the fifth and sixth cycle (see Figure 7). In contrast, the tensile strength of BioMed Clear V1 remains consistently high across all autoclaving cycles (see Figure 7), indicating good suitability for repeated steam sterilization. The strain at break decreases in all specimens with an increasing number of autoclaving cycles, indicating increased brittleness and aligning with expectations. Notably, the strain of Black V4 ($10.1 \pm 0.6\%$) after 10 autoclaving cycles still exceeds the manufacturer's specification of 6.2%, suggesting that the material retains a comparatively higher ductility even after repeated sterilization. This relatively low reduction in brittleness may help explain the more stable tensile strength observed for Black V4. In contrast, for Clear V4, where tensile strength decreases noticeably after 10 autoclaving cycles, the strain at break approaches the manufacturer's reported value, indicating increased brittleness and a corresponding loss in mechanical performance.

The test series indicates that repeated autoclaving has no measurable influence on the Young's modulus under the applied testing conditions. However, the absolute Young's modulus values obtained in this study are not directly comparable to the manufacturer's data, as they are based on different testing standards and evaluation methods. While Formlabs reports Young's modulus values determined according to ASTM D638, the present study follows DIN EN ISO 527-1.

The key methodological difference between these standards lies in the definition of Young's modulus. ASTM D638 determines the Young's modulus based on a local, point-wise evaluation of the initial slope of the stress–strain curve at very small strains, whereas DIN EN ISO 527-1 defines the Young's modulus as a secant modulus over a standardized low-strain interval. For polymeric materials exhibiting nonlinear and viscoelastic behavior at small strains, this fundamental difference in evaluation approach leads to systematic deviations in the calculated Young's modulus, although the underlying stress–strain data remain unchanged. Consequently, the Young's modulus should be regarded as a norm-specific parameter.

By contrast, tensile strength and strain-related values are derived from the macroscopic stress–strain response at higher deformation levels and are therefore much less sensitive to differences in the evaluation of the initial elastic region. As a result, tensile strength and elongation values obtained according to DIN and ASTM standards are generally more comparable than Young's modulus values.

It should be emphasized that the objective of this study was not to reproduce manufacturer-provided material data, but to

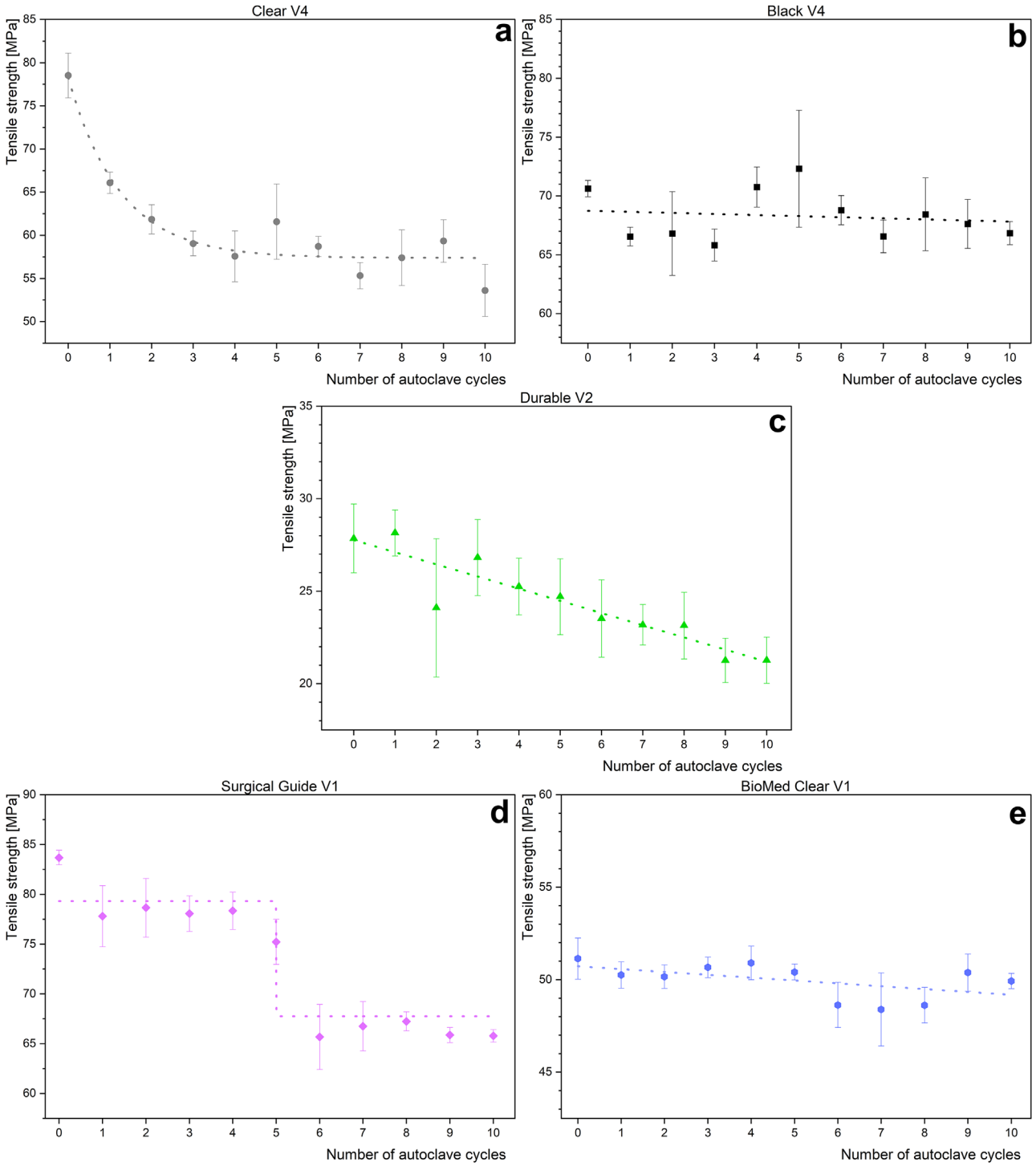

FIGURE 7 | Measured tensile strength of resin-based specimens autoclaved 0 to 10 times, including trend lines. The tested materials were (a) Clear V4, (b) Black V4, (c) Durable V2, (d) Surgical Guide V1, and (e) BioMed Clear V1. For each condition, at least five replicates were tested according to DIN EN ISO 527-2. Error bars represent the standard deviation.

evaluate the influence of repeated autoclaving on key mechanical properties. As all tests were conducted under identical and controlled conditions, the results demonstrate that autoclaving does not significantly affect the Young's modulus within the investigated parameter range.

Regarding other mechanical properties, none of the specimens were physically damaged during the autoclaving process. However, tensile testing revealed a pronounced increase in brittleness of the High Temp material, rendering it unsuitable for the intended application. Among the officially non-biocompatible materials, the Black V4 specimens retained the highest tensile strength after 10 autoclaving cycles, demonstrating the most stable tensile strength throughout the tests. When comparing the two biocompatible materials, it is notable that Surgical Guide exhibited a higher tensile strength, even after 10 autoclaving

TABLE 2 | Tensile test results of the investigated materials after 0, 1, 5, and 10 autoclaving cycles, including comparison with manufacturer specifications (marked grey) where available.

Specimen (number of autoclave cycles)	Specification: Tensile strength [MPa]	Measured tensile strength [MPa]	Specification strain at break [%]	Measured strain at break [%]	Specification: Young's modulus [MPa]	Measured young's modulus [MPa]
Clear V4 (0)	65	78.5 ± 2.6	6.2	9.7 ± 0.8	2800	682 ± 15
Clear V4 (1)	—	66.0 ± 1.2	—	8.7 ± 1.8	—	765 ± 19
Clear V4 (5)		61.6 ± 4.4		8.3 ± 1.1		693 ± 80
Clear V4 (10)		53.6 ± 3.0		6.3 ± 0.7		697 ± 52
Clear V5 (0)	60	72.7 ± 0.7	8	9.4 ± 1.5	2750	738 ± 17
Black V4 (0)	65	70.6 ± 0.7	6.2	16.5 ± 2.2	2800	721 ± 14
Black V4 (1)	—	66.6 ± 0.8	—	12.9 ± 0.7	—	754 ± 94
Black V4 (5)		72.3 ± 4.9		8.5 ± 1.4		728 ± 38
Black V4 (10)		66.9 ± 0.9		10.1 ± 0.6		743 ± 78
Black V5 (0)	61	63.3 ± 0.6	10	10.7 ± 1.9	2700	737 ± 14
High Temp V2 (0)	58.3	63.4 ± 6.4	3.3	5.9 ± 0.9	2800	867 ± 67
High Temp V2 (5)	—	20.3 ± 2.9	—	2.2 ± 0.5	—	993 ± 33
Durable V2 (0)	28	27.8 ± 1.9	55	52.0 ± 5.4	1000	414 ± 27
Durable V2 (1)	—	28.14 ± 1.2	—	49.5 ± 4.3	—	429 ± 31
Durable V2 (5)		24.7 ± 2.0		52.3 ± 6.5		401 ± 13
Durable V2 (10)		21.3 ± 1.3		36.1 ± 4.1		491 ± 11
Surgical Guide V1 (0)	—	83.7 ± 0.7	12	12.9 ± 2.9	—	765 ± 82
Surgical Guide V1 (1)		77.8 ± 3.1	—	9.9 ± 2.1		778 ± 31
Surgical Guide V1 (5)		75.2 ± 2.3		10.6 ± 0.6		750 ± 20
Surgical Guide V1 (10)		65.8 ± 0.6		10.0 ± 1.5		731 ± 9
BioMed Clear V1 (0)	52	51.1 ± 1.1	12	15.6 ± 1.3	2080	648 ± 42
BioMed Clear V1 (1)	—	50.3 ± 0.7	—	10.1 ± 2.5	—	666 ± 20
BioMed Clear V1 (5)		50.4 ± 0.4		8.9 ± 0.1		700 ± 17
BioMed Clear V1 (10)		49.9 ± 0.4		7.3 ± 0.3		671 ± 13

cycles, although its tensile strength dropped sharply after five cycles. In contrast, BioMed Clear Resin displayed a lower initial tensile strength than Surgical Guide Resin, but remained relatively constant throughout all autoclaving cycles. For the purposes of this study, the number of autoclaving cycles was limited to a maximum of 10. The results suggest that the five materials shown in Figure 7 retain their mechanical strength after 10 autoclave cycles and may therefore be suitable for repeated autoclaving beyond the number of cycles investigated in this study.

3.3 | TOC evaluation as an Indicator of Potential Leachables From 3D-Printed Resins

A total organic carbon (TOC) analysis was performed to identify potential leachables from the resin materials. The TOC concentrations in mg/L for the three autoclaving cycles are shown in Figure 8. With the exception of High Temp and BioMed Clear, the TOC levels are relatively high after the first autoclaving and decrease significantly after the second cycle. A notable difference

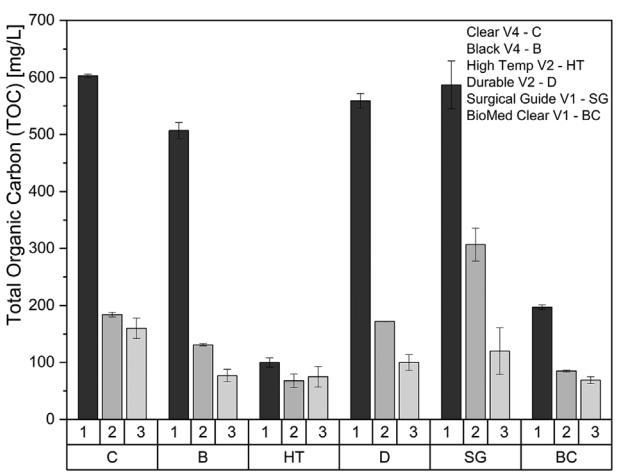

FIGURE 8 | Total organic carbon (TOC) content in mg/L of resin materials after 1–3 autoclaving cycles at 121°C, 2 bar, for 30 min. For each material, three replicates were measured. Error bars indicate standard deviation. The surface-to-volume ratio during testing was 1071.3 mm^2/mL.

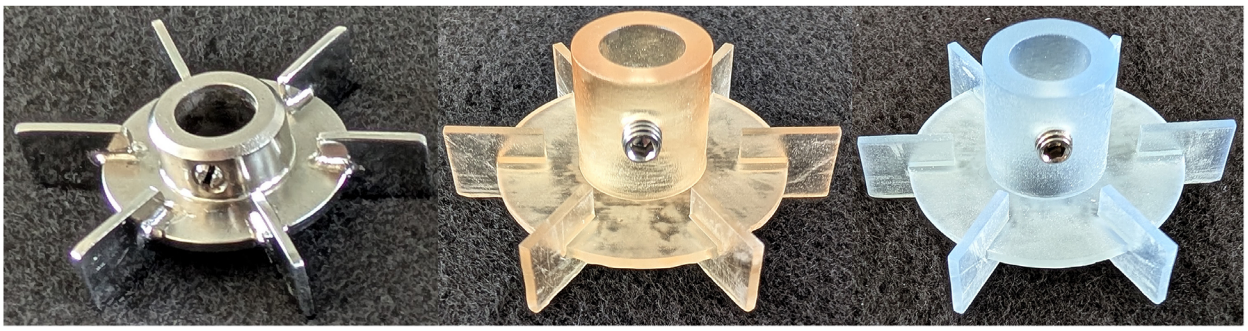

FIGURE 9 | Rushton turbines for fermenter application: Metal (left), Surgical Guide (center), and BioMed Clear (right).

between the second and third cycle is only observed for Surgical Guide. For the other materials, it can be assumed that most contamination is released into the medium during the first autoclaving cycle.

The low TOC value for High Temp may be attributed to the material's high thermal stability. According to the manufacturer, it remains stable up to 238°C after specific post-treatment, while Clear is only rated up to 73°C, but in practice shows a higher temperature load capacity. It is also conceivable that the particular resin formulation of high temp, potentially containing a higher proportion of short-chain components, results in reduced release of degradation products under thermal stress. However, this remains speculative, as detailed information on the exact chemical composition and degradation behaviour of the resin is not publicly available. A similar trend of decreasing concentrations was also observed in an LC-MS analysis (data not shown here), where the intensity of a detected peak—presumably originating from a polymer—decreased with increasing autoclaving cycles. However, since the exact composition of the resins is unknown, such analytical evaluations remain challenging. Additionally, it remains unclear whether the released breakdown products pose any risk to microorganisms.

3.4 | Influence of 3D-Printed Components on Fermentation Performance

To examine how 3D printing materials affect fermentation processes, Rushton turbines (RTs) with the same diameter as standard metal stirrers used in fermenters (0.4 D, where D = 130 mm) were designed and printed from two biocompatible materials, Surgical Guide and BioMed Clear (Figure 9). The specific surface area of the 3D printed materials in relation to the fermenter volume (5702.9 mm^2/1.5 L = 3.8 mm^2/mL) is by a factor of about 268 significantly lower compared to the corresponding specific surface area in the microtiter plate experiments described in section 3.1 (1071.3 mm^2/1 mL = 1071.3 mm^2/mL). Therefore, a material-related influence on the microorganisms in the fermenter seems even less likely than what was already shown in the microtiter plate experiments. Each fermentation in the fermenter involved testing a two-stage RT–RT configuration with installation heights set at 1/3 and 2/3 of the total working height (130 mm).

The fermentation data are presented in Figures 10–13. First, the effect on the growth curve was examined by measuring the optical

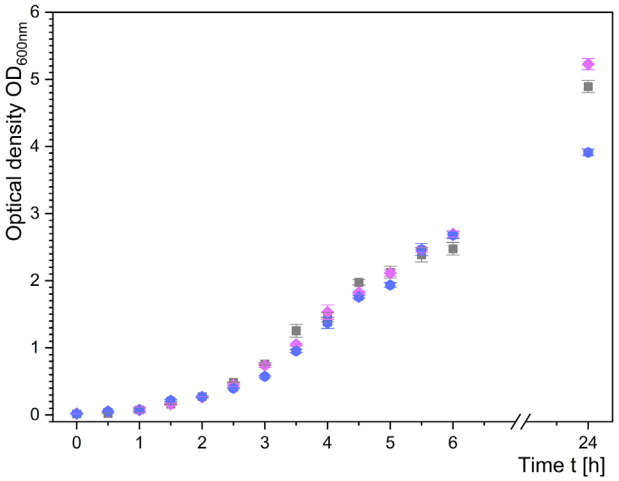

FIGURE 10 | Growth curve of *E. coli* fermentations over 24 h using two-stage Rushton turbines made from (1) metal, (2) Surgical Guide resin, and (3) BioMed Clear resin. For each material, three replicates were performed. Error bars indicate standard deviation.

density at 600 nm during the first 6 h after the start of fermentation and after 24 h. During the initial 6 h, slight fluctuations in OD values were observed among the three fermentations; however, their overall behaviour was very similar. After 24 h, the BioMed Clear Rushton turbine fermentation exhibited a lower OD than the other two. While optical density is an important parameter, understanding this deviation also requires examining protein concentration (Figure 11) and substrate concentration (Figure 12).

The protein concentration in the BioMed Clear fermentation was slightly lower after 24 h compared to the other two. However, this difference is minimal and likely due to natural biological variation in microbial growth. Analyzing the substrate concentration over time reveals that it remained higher throughout the BioMed Clear fermentation, suggesting slower substrate metabolism by the organisms. Nonetheless, it is unlikely that the 3D printing material directly causes this. When viewed in isolation, the substrate concentration profile in the BioMed Clear fermentation appears natural and plausible. Only in direct comparison with the other two fermentations does it stand out as noticeably higher, which could account for the lower optical density, as less substrate was metabolized to support cell growth.

After fermentation, specific enzymatic activities of the harvested β-galactosidase were determined and compared (Figure 13).

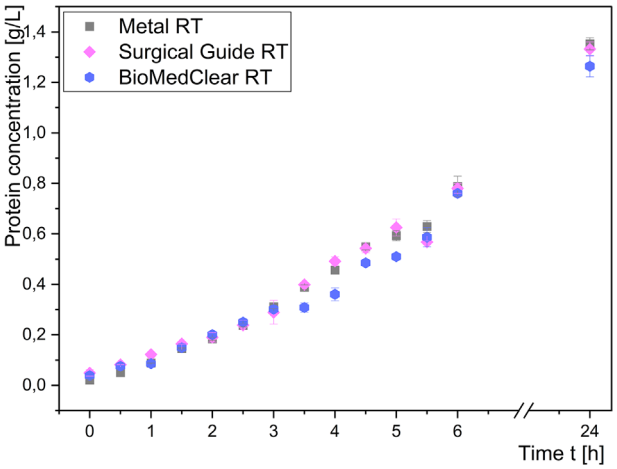

FIGURE 11 | Protein concentrations of an *E. coli* fermentation over 24 h using two-stage Rushton turbines made from (1) metal, (2) Surgical Guide resin, and (3) BioMed Clear resin. Protein concentrations were determined using the Bradford assay. For each material, three replicates were performed. Error bars indicate standard deviation.

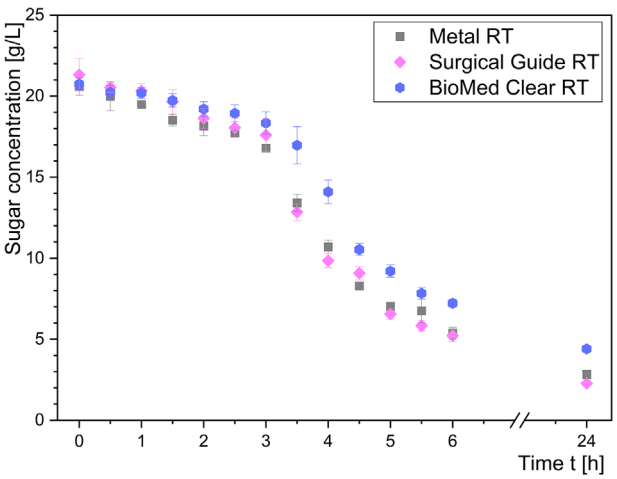

FIGURE 12 | Substrate concentrations (lactose concentrations) of *E. coli* fermentations over 24 h using Rushton turbines made from (1) metal, (2) Surgical Guide resin, and (3) BioMed Clear resin. Measurements were performed using the DNS assay. For each material, three replicates were performed. Error bars indicate standard deviation.

When comparing the results of the specific enzymatic activities, it is important to note that the values from the BioMed Clear fermentation (0.78 mol/h/g), despite the lower OD, are very similar to those from the fermentation using the metal stirrer (0.79 mol/h/g). The higher enzymatic activity (~20%) observed in the fermentation with Surgical Guide stirrers (0.95 mol/h/g) can be attributed to natural variation, as all other fermentation parameters and the stirrer diameters were identical.

Overall, the results of the fermentations show that internal components made from 3D-printed resin materials can be effectively utilized in microbial fermentation processes. The effects of a 3D-printed stirrer as an example of 3D-printed, autoclavable, inexpensive and reusable components on the growth of microorganisms in these series of experiments appear to be negligible and

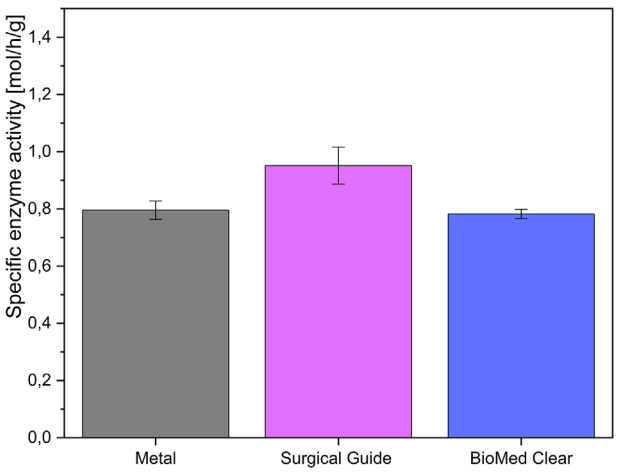

FIGURE 13 | Specific enzymatic activity of β-galactosidase harvested after 24-h *E. coli* fermentations using two-stage Rushton turbines made from (1) metal, (2) surgical guide resin, and (3) BioMed clear resin. Enzymatic activity was photometrically determined using the ONPG assay. For each material, three replicates were performed. Error bars indicate standard deviation.

insignificant to nonexistent. This exemplifies significant potential for design studies and research into various stirrer designs in fermentation, which would otherwise require considerably greater effort if constructed from metal. The reuse of autoclavable 3D equipment represents a way to increase sustainability in laboratory and pilot plant processes.

4 | Concluding Remarks

In summary, this study shows a successful method development in different scales for evaluating the usability of different 3D printing materials in biotechnological applications and possible effects on microbial metabolic processes. It could be proven that using autoclavable 3D printing materials in biotechnology applications appears feasible and recommendable. In the case of both a native and a genetically modified *E. coli* strain, no deviations in key parameters were observed in either the MTP assay or the fermentation process that could be directly linked to the 3D printed materials. It has been demonstrated that there is no need to fear that the growth of the microorganisms examined is significantly influenced by microparticles or components released from the printing material.

Extensive tensile tests of the various materials successfully demonstrated that, except for the material High Temp, all tested materials were generally suitable for at least, but probably significantly more than 10 autoclaving cycles, as none showed total structural failure due to the autoclaving process, and the strength values obtained were still within a satisfactory range. The in-house measurement method for tensile tests can be considered successfully verified based on comparable manufacturer data. However, the resulting data appear to be more differentiated, and a temporal development could also be provided. The data base provided in this study closes a research gap, and it expands the current state of knowledge and the application-oriented potential technical uses. The material Black V4 is particularly promising.

Although not explicitly labelled as autoclavable by the manufacturer, it exhibited no significant changes in tensile strength even after 10 autoclaving cycles. Additionally, this material did not show any growth-inhibiting effects in the MTP assay with native *E. coli*. Given that the surface-to-volume ratio in the fermenter is significantly lower, the material also appears very promising for use in fermentation processes. While further testing is still necessary, the results suggest that the use of certified biocompatible materials, which tend to be significantly more expensive, may not always be required, depending on the application. TOC analysis revealed that most of the potentially toxic compounds are released from the material into the medium during the first autoclaving cycle, with a marked reduction occurring during the second and third cycles. Therefore, performing an initial autoclaving step before actual use in systems such as bioreactors is recommended to ensure that leachables and soluble organic components from the 3D-printed materials are washed out or that any residual monomers are polymerized and fixed.

To draw broader conclusions about the use of 3D-printed resin materials in biotechnology, additional microorganisms need to be tested. This research concentrated on *E. coli*, a key microorganism in both industry and research. The findings suggest that these resins are applicable for such uses and that multiple autoclaving cycles can be performed, potentially enhancing the integration of various laboratory workflows in biotechnology. Furthermore, because 3D-printed stirrers can operate in fermenters without producing toxic effects on fermentation, this method presents noteworthy research possibilities and design optimization studies. The adaptability of 3D printing enables quick and easy manufacturing of stirrers and equipment in different shapes and sizes, allowing for flexible designs in fermenter examinations. Further studies, including measurements of k_La values, which represent the volumetric mass transfer coefficient and indicate the efficiency of oxygen transfer from the gas to the liquid phase, or assessments of shear forces for varying 3D-printed stirrer designs, could yield more information regarding their effectiveness and impact on fermentation processes.

Acknowledgments

The authors acknowledge the financial support through the Federal Ministry for Economic Affairs and Energy (project number 22782 N/1). Financial support by Project DEAL is gratefully acknowledged.

Open access funding enabled and organized by Projekt DEAL.

Funding

The project on which this article is based was funded by the Federal Ministry for Economic Affairs and Energy under the number "22782 N/1".

The responsibility for the content of this publication lies with the author.

Ethics Statement

This research did not require ethics approval, as it did not involve any experiments on humans or animals. Consequently, no patient consent statement or clinical trial registration is necessary.

Conflicts of Interest

The authors declare no conflicts of interest.

Data Availability Statement

The authors confirm that the data supporting the findings of this study are available within the article [and/or] its supplementary materials.

Permission to Reproduce Material From Other Sources

All necessary permissions have been obtained by providing the actual written permission granted by the copyright owner.

References

1. A. Jadhav and V. S. Jadhav, "A Review on 3D Printing: An Additive Manufacturing Technology," *Materials Today: Proceedings* 62, no. 4 (2022): 2094–2099, https://doi.org/10.1016/j.matpr.2022.02.558.

2. H. Quan, T. Zhang, H. Xu, S. Luo, J. Nie, and X. Zhu, "Photo-Curing 3D Printing Technique and Its Challenges," *Bioactive Materials* 5 (2020): 110–115, https://doi.org/10.1016/j.bioactmat.2019.12.003.

3. P. Kumar, D. K. Rajak, M. Abubakar, S. G. M. Ali, and M. Hussain, "3D Printing Technology for Biomedical Practice: A Review," *Journal of Materials Engineering and Performance* 30 (2021): 5342–5355, https://doi.org/10.1007/s11665-021-05792-3.

4. G. M. Tartaglia, A. Mapelli, C. Maspero, et al., "Direct 3D Printing of Clear Orthodontic Aligners: Current State and Future Possibilities," *Materials* 14, no. 7 (2021): 1799, https://doi.org/10.3390/ma14071799.

5. M. Savastano, C. Amendola, F. D'Ascenzo, and E. Massaroni, "3-D Printing in the Spare Parts Supply Chain: An Explorative Study in the Automotive Industry," in *Digitally Supported Innovation. Lecture Notes in Information Systems and Organisation*, ed. L. Caporarello, F. Cesaroni, R. Giesecke, and M. Missikoff, (Springer, 2016), https://doi.org/10.1007/978-3-319-40265-9_11.

6. C. Heuer, J. A. Preuß, T. Habib, A. Enders, and J. Bahnemann, "3D Printing in Biotechnology—An Insight Into Miniaturized and Microfluidic Systems for Applications From Cell Culture to Bioanalytics," *Engineering in Life Sciences* 22 (2021): 744–759, https://doi.org/10.1002/elsc.202100081.

7. P. Satzer and L. Achleitner, "3D Printing: Economical and Supply Chain Independent Single-Use Plasticware for Cell Culture," *New Biotechnology* 69 (2022): 55–61, https://doi.org/10.1016/j.nbt.2022.03.002.

8. L. Achleitner, M. Winter, and P. Satzer, "3D Printed Autoclavable Biocompatible Biodegradable Bioreactor Vessels With Integrated Sparger Made From Poly-Lactic Acid," *Journal of Biotechnology* 391 (2024): 33–39, https://doi.org/10.1016/j.jbiotec.2024.06.001.

9. T. H. Lücking, F. Sambale, B. Schnaars, D. Bulness-Abundis, S. Beutel, and T. Scheper, "3D-Printed Individual Labware in Biosciences by Rapid Prototyping: In Vitro Biocompatibility and Applications for Eukaryotic Cell Cultures," *Engineering in Life Sciences* 15 (2015): 57–64, 10.1002/elsc.201400094.

10. Y. Song, Y. Ghafari, A. Asefnejad, and D. Toghraie, "An Overview of Selective Laser Sintering 3D Printing Technology for Biomedical and Sports Device Applications: Processes, Materials, and Applications," *Optics & Laser Technology* 171 (2024): 110459, https://doi.org/10.1016/j.optlastec.2023.110459.

11. F. E. Jabri, A. Ouballouch, L. Lasri, and R. E. Alaiji, "A Comprehensive Review of Polymer Materials and Selective Laser Sintering Technology for 3D Printing," *Journal of Achievements in Materials and Manufacturing Engineering* 118 (2023): 5–17, https://doi.org/10.5604/01.3001.0053.7286.

12. Markforged, ROI for metal 3D printers (2023), https://markforged.com/resources/blog/roi-for-metal-3d-printers.

13. Z. Chen, Z. Li, J. Li, et al., "3D Printing of Ceramics: A Review," *Journal of the European Ceramic Society* 39, no. 4 (2019): 661–687, https://doi.org/10.1016/j.jeurceramsoc.2018.11.013.

14. M. Matzke, M. Ulbricht, and H. J. Schultz, "Investigation of the Mixing Time Distribution and Connected Flow Fields in Two-Stage Stirred Vessels," *Processes* 12, no. 1 (2024): 132, https://doi.org/10.3390/pr12010132.

15. M. Matzke, C. Behrens, N. Jongebloed, D. Steins, M. Ulbricht, and H. J. Schultz, "Investigation and Visualization of Flow Fields in Stirred Tank Reactors Using a Fluorescence Tracer Method," *Chemie Ingenieur Technik* 94, no. 8 (2022): 1131–1140, https://doi.org/10.1002/cite.202200006.

16. M. Matzke, L. Mussial, N. Jongebloed, M. Ulbricht, and H. J. Schultz, "Power Characteristics of Unconventional 3D-Printed Impellers," *Chemie Ingenieur Technik* 94, no. 9 (2022): 1357, https://doi.org/10.1002/cite.202255303.

17. S. Kreß, R. Schaller-Ammann, J. Feiel, J. Priedl, C. Kasper, and D. Egger, "3D Printing of Cell Culture Devices: Assessment and Prevention of the Cytotoxicity of Photopolymers for Stereolithography," *Materials* 13, no. 13 (2020): 3011, 10.3390/ma13133011.

18. R. P. Rimington, A. J. Capel, D. J. Player, R. J. Bibb, S. D. R. Christie, and M. P. Lewis, "Feasibility and Biocompatibility of 3D-Printed Photopolymerized and Laser Sintered Polymers for Neuronal, Myogenic, and Hepatic Cell Types," *Macromolecular Bioscience* 18, no. 7 (2018), https://doi.org/10.1002/mabi.201800113.

19. I. G. Siller, A. Enders, T. Steinwedel, et al., "Real-Time Live-Cell Imaging Technology Enables High-Throughput Screening to Verify in Vitro Biocompatibility of 3D Printed Materials," *Materials* 12 (2019): 2125, https://doi.org/10.3390/ma12132125.

20. N. Pradeep and A. V. Sreekumar, "An In Vitro Investigation Into the Cytotoxicity of Methyl Methacrylate Monomer," *The Journal of Contemporary Dental Practice* 13, no. 6 (2012): 838–841, https://doi.org/10.5005/jp-journals-10024-1239.

21. H. B. Musgrove, M. A. Catterton, and R. R. Pompano, "Applied Tutorial for the Design and Fabrication of Biomicrofluidic Devices by Resin 3D Printing," *Analytica Chimica Acta* 1209 (2022): 339842, https://doi.org/10.1016/j.aca.2022.339842.

22. M. E. Walsh, A. Ostrinskaya, M. T. Sorensen, D. S. Kong, and P. A. Carr, "3D-Printable Materials for Microbial Liquid Culture," *3D Printing and Additive Manufacturing* 3 (2016): 113–118, https://doi.org/10.1089/3dp.2016.0007.

23. Deutsches Institut für Normung. Kunststoffe—Bestimmung der Zugeigenschaften Teil 1: Allgemeine Grundsätze, Beuth-Verlag, (2019).

24. Deutsches Institut für Normung. Kunststoffe—Bestimmung der Zugeigenschaften Teil 2: Prüfbedingungen für Form- und Extrusionsmassen, Beuth-Verlag, (2012).

25. O. Tuteski and A. Kočov, "Tensile Strength and Dimensional Variances in Parts Manufactured by Sla 3D Printing," *Industry 4.0* 6 (2021): 143–149.

Supporting Information

Additional supporting information can be found online in the Supporting Information section.

Supporting File: elsc70076-sup-0001-SuppMat.docx.